

The Disk Substructures at High Angular Resolution Project (DSHARP) III: Spiral arms observed in the millimeter continuum of the Elias 27, IM Lup, and WaOph 6 protoplanetary disks

JANE HUANG¹ AND OTHERS

¹*Harvard-Smithsonian Center for Astrophysics, 60 Garden Street, Cambridge, MA 02138, USA*

ABSTRACT

We present an analysis of ALMA 1.3 millimeter continuum observations of spiral arm structures in three protoplanetary disks hosted by single stars from the Disk Substructures at High Angular Resolution Project (DSHARP). The Elias 27, IM Lup, and WaOph 6 disks feature $m = 2$ trailing spiral patterns combined with axisymmetric gap and ring structure. The spiral pattern in the Elias 27 disk extends throughout much of the Elias 27 disk, and the arms cross the annular gap located at a radius of ~ 70 AU. The spiral pattern in the IM Lup disk extends about halfway radially through the disk and is highly complex, exhibiting pitch angle variations with radius and the presence of either additional ring structures intersecting the arms or “spurs” branching off the arms. comparatively compact and features pitch angle variations with radius. Spiral arms extend most of the way through the WaOph 6 disk, but the source overall is much more compact than the other two disks. We discuss possible scenarios for the origin of these arms, including gravitational instability and companion-induced spiral density waves.

Keywords: protoplanetary disks—ISM: dust—techniques: high angular resolution

1. INTRODUCTION

Over the past decade and a half, spiral arms have been detected in scattered light in a number of protoplanetary disks (e.g. Fukagawa et al. 2004; Muto et al. 2012; Grady et al. 2013; Dong et al. 2018a). The origins of these features are highly debated—proposed mechanisms for inducing spiral features include perturbations by a companion (e.g. Goldreich & Tremaine 1979; Tanaka et al. 2002), gravitational instability (e.g. Mayer et al. 2004; Lodato & Rice 2004), and pressure variations due to shadowing (e.g. Montesinos et al. 2016; Montesinos & Cuello 2018).

Scattered light observations trace the distribution of small grains in the upper layers of protoplanetary disks, but do not probe the disk midplane.

etc

The Disk Substructures at High Angular Resolution Project (Andrews et al. in prep, henceforth DSHARP1), undertook a high angular resolution 1.3 mm continuum survey of 20 protoplanetary disks with ALMA. Spiral features were observed in five of these disks: Elias 27, IM Lup, WaOph 6, HT Lup, and AS 205. The four new spiral detections thus bring up the total number of disks with spiral arms detected in millimeter continuum to six. HT Lup and AS 205 are in binary disk systems

and are discussed further in Kurtovic et al. (in prep). The present paper focuses on spiral structures detected in the single protoplanetary disk systems Elias 27, IM Lup, and WaOph 6. Section 2 provides an overview of the sample and the observations. Section 3 provides an analysis of the spiral properties. Section 4 places the targets analyzed in this work in the context of other spiral arm observations and discusses possible origins for the arms. Section 5 summarizes the findings.

2. SOURCE PROPERTIES AND OBSERVATIONS

Elias 27 is an 800,000-year-old M0 star located 116 pc away in the ρ Oph star-forming region (Luhman & Rieke 1999; Gaia Collaboration et al. 2018). The first detection of spiral arms in millimeter continuum was in the disk hosted by Elias 27 (Pérez et al. 2016). IM Lup is a 500,000-year-old K5 star located 158 pc away in the Lupus II cloud (Alcalá et al. 2017; Gaia Collaboration et al. 2018). Both the gas disk as traced by ^{12}CO and dust disk as traced by millimeter continuum and scattered light are unusually large in radial extent (e.g Pinte et al. 2008; Cleeves et al. 2016; Avenhaus et al. 2018). Finally, WaOph 6 is a 300,000-year-old K6 star located 123 pc away in ρ Ophiuchus (Eisner et al. 2005; Gaia Collaboration et al. 2018).

The three disks also have gap and ring structures that are discussed in more detail in DSHARP2. We refer to these structures throughout the paper using the same nomenclature, e.g. DA70 refers to a dark annulus at a

Corresponding author: Jane Huang
jane.huang@cfa.harvard.edu

radius of 70 AU, and BR87 refers to a bright ring at a radius of 87 AU.

The observational setup and data calibration are described in DSHARP1, and the imaging procedure is described in Huang et al. (in prep), hereafter DSHARP2. The Elias 27, IM Lup, and WaOph 6 protoplanetary disks were observed at angular resolutions ranging from ~ 40 to ~ 60 mas, corresponding to scales of ~ 6 or 7 AU. Because of the diffuse and relatively low SNR emission in the outer regions of the Elias 27 disk, we also incorporate in our analysis an image of Elias 27 created by applying a gaussian *uv* taper that increases the SNR and results in a synthesized beam of 85 mas \times 81 mas (-75°.1).

3. DISK FEATURES

3.1. Overview of spiral morphology

Figure 1 shows the 1.3 millimeter continuum images of the Elias 27, IM Lup, and WaOph 6 disks as well as maps of the intensity distribution as a function of polar angle and radius in deprojected coordinates. The inclinations and position angles used for deprojection are taken from DSHARP2. In the polar angle-radius plots, axisymmetric structure (i.e., gaps and rings) manifest as light or dark vertical bands. The spiral structures manifest as bright emission bands crossing the polar angle-radius plots diagonally. The spiral patterns in each disk can be observed more readily by subtracting an axisymmetric intensity profile from the disk image (Figure 2). The axisymmetric profile is derived by deprojecting the disk, binning the pixels in AU-wide annuli centered at the continuum peak, and finding the median pixel intensity in each bin.

All of the disks appear to be dominated by an $m = 2$ spiral pattern (i.e., two-fold rotational symmetry). The spiral pattern in the Elias 27 disk extends from $R \sim 50$ AU to $R \sim 230$ AU, nearly the full detectable extent of the millimeter continuum emission. Based on the polar angle-radius plot in Figure 2, the pattern wraps at least $\sim 225^\circ$ around the disk. The new high-resolution observations demonstrate that the spiral pattern extends at least several tens of AU further inward than what was visible in previous observations by Pérez et al. (2016). It can now be seen that the spiral pattern intersects DA87, as shown in the first columns of Figures 1 and 2.

Although the overall radial extent of the IM Lup disk is comparable to that of Elias 27, the spiral pattern appears to be confined to a more compact region extending from $R \sim 25$ to ~ 110 AU, nested inside the gap/ring pair DA118/BR133. The pattern appears to wrap $\sim 270^\circ$ around the disk. However, there appears to be additional substructure just exterior to BR133 in the IM Lup disk that may be another pair of spiral arms, a continuation of the interior spiral arms, or a ring that is not well-resolved along the minor axis (see Figure 3). Observations with better angular resolution and signal-

to-noise will be necessary to confirm the nature of these substructures.

Both the overall millimeter continuum emission extent and extent of the spiral pattern are more compact for the WaOph 6 disk compared to Elias 27 and IM Lup. The spiral pattern extends from $R \sim 25$ to 75 AU, nested inside the gap/ring pair DA80/BR88. The azimuthal extent of the pattern appears to be $\sim 220^\circ$.

Figure 2 shows apparent discontinuities in the spiral arms at $R \sim 75$ AU for IM Lup and $R \sim 50$ AU for WaOph 6. The appearance of a discontinuity arises when the emission is axisymmetric (or nearly so). At the radii corresponding to the discontinuities, additional substructures that are not part of the main spiral arms can be identified, as shown in Figure 4. These substructures could be additional ring structures, with each disk having either a pair of spiral arms that crosses a bright emission ring or two pairs of spiral arms separated by a bright emission ring. Another possibility is that the substructures present at $R \sim 75$ AU for IM Lup and $R \sim 50$ AU for WaOph 6 are “spurs” off the main spiral arms, like those observed sometimes in spiral galaxies (e.g. Elmegreen 1980).

For each of these disks, it is possible that the main spiral arms extend further inward and outward than what is noted. Spirals in the outermost regions of the disk would be difficult to measure due to the low signal-to-noise. In the inner few tens of AU in the disk, spiral arms could also be difficult to detect due to distortions imposed by the PSF and insufficient intensity contrasts in optically thick regions.

3.2. Absolute geometry of the disk systems from ^{12}CO emission

(Author note: Sean still needs to put the ^{12}CO images in)

The optically thick ^{12}CO $J = 2 - 1$ line observations in each disk in DSHARP1 enable the absolute geometry of each disk to be determined. The three sources have relatively high inclinations and visibly flared CO emission, allowing the near side of the disk to be identified because the far side appears brighter and foreshortened (e.g. Rosenfeld et al. 2013). CO observations toward the disk indicate that the southwest side of the disk is the near side, with blueshifted emission originating northwest of the disk center and the redshifted emission originates from the southeast. Scattered light observations of the IM Lup disk also indicate that the southwest side is the near side (Avenhaus et al. 2018). The ^{12}CO $J = 2 - 1$ emission in the Elias 27 disk appears to exhibit geometry similar to that of IM Lup, as discussed previously in Pérez et al. (2016), although foreground cloud contamination creates some ambiguity in the identification of the near side. Finally, WaOph 6 appears to be inclined such that the east side is tilted toward the observer, with the blueshifted emission originating north of the disk center and the redshifted emission from the

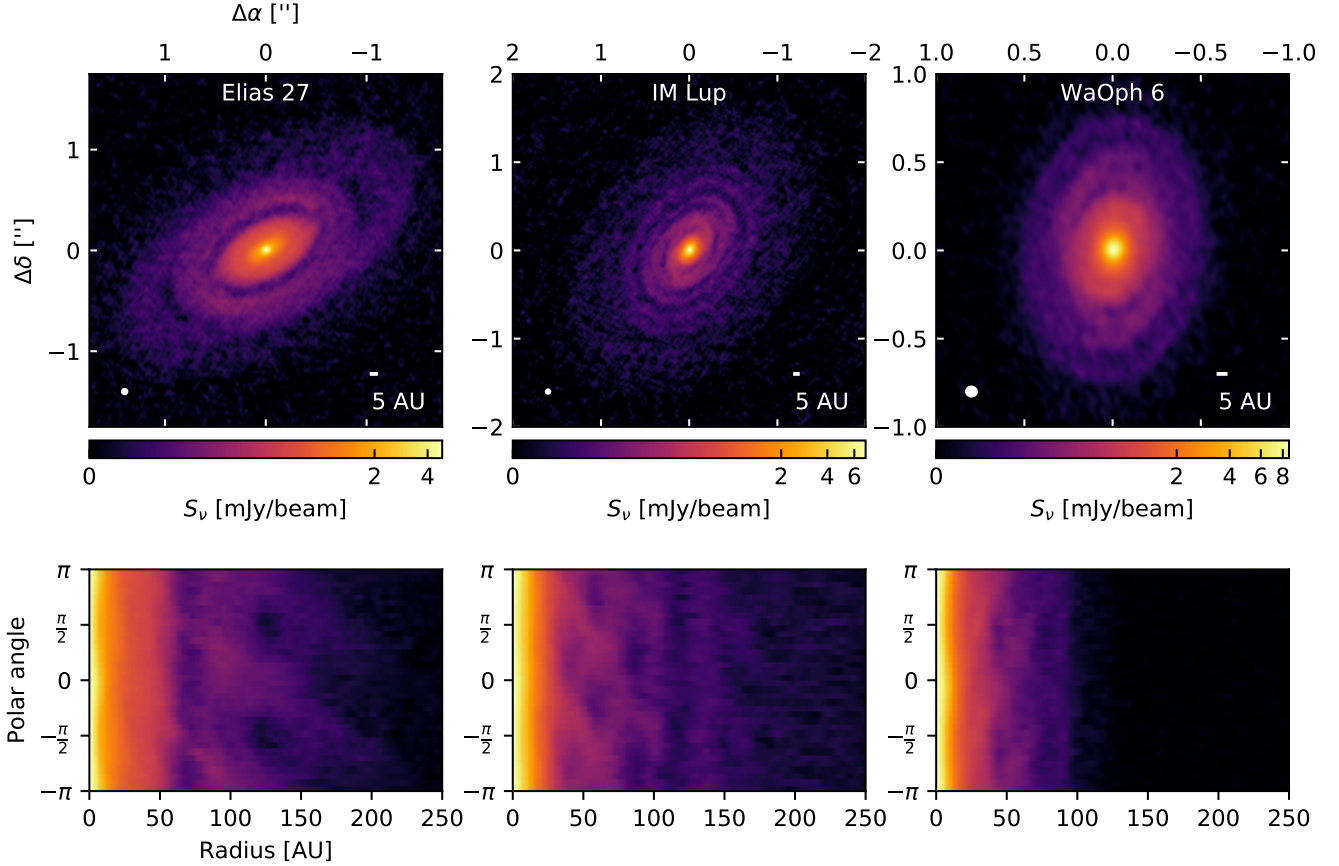


Figure 1. *Top:* ALMA 1.3 mm continuum images of the Elias 27, IM Lup, and WaOph 6 disks. The respective synthesized beam is shown in the lower left corner of each panel. *Bottom:* The 1.3 mm continuum emission deprojected and replotted as a function of radius and polar angle.

south. Thus, for all three sources, the spiral arms appear to be trailing (i.e., the outer ends point opposite to the direction of rotation).

3.3. Spiral arm pitch angles

Adopting a procedure based on Pérez et al. (2016), the radial positions of the spiral arms in each disk as a function of (deprojected) polar angle are determined by deprojecting the dust continuum image, subtracting the median radial intensity profile, and locating the radius at which local maxima occur along a scanline of constant θ . The uncertainties in R are assumed to be Gaussian, with the 1σ uncertainty estimated to be equal to the standard deviation along the major axis of the synthesized beam, adjusted for deprojection (i.e., in deprojected coordinates, the uncertainties in R along the minor axis of the projected disk image are larger than along the major axis because the minor axis is not as well-resolved).

Each spiral feature is first modeled as a logarithmic spiral, which has the form $R(\theta) = R_0 e^{b\theta}$, where θ is the polar angle in radians. The pitch angle of a spiral is $\mu = \arctan \left| \frac{d \log r}{d\theta} \right|$, so the pitch angle of a logarithmic spiral is simply $\mu = \arctan |b|$. For spiral arms that cross the 180° boundary, the polar angles are phase-unwrapped before fitting to eliminate the 2π jump. The geometry of each arm is measured independently in order to assess whether the pitch angles vary between arms in the same disk. A Gaussian likelihood is specified and flat priors are adopted for R_0 and b . The posterior probabilities are explored via the affine invariant MCMC sampler as implemented in `emcee` (Goodman & Weare 2010; Foreman-Mackey et al. 2013). The ensemble, consisting of 40 walkers, is evolved for 15,000 steps. Convergence of the MCMC chains is evaluated by checking that the number of steps significantly exceeded the autocorrelation time (generally less than 10^2 steps).

To explore the possibility of a pitch angle that varies with radius, we also fit the features with Archimedean spirals, which take the form $R(\theta) = a + c\theta$. The pitch angle is then $\mu = \frac{c}{R}$ (i.e., the pitch angle decreases with radius). More complex expressions have been developed for the shapes of spiral wakes in protoplanetary disks (e.g. Rafikov 2002; Zhu et al. 2015), but given that none of the spiral features are detected for more than a full winding, which would be key for distinguishing between

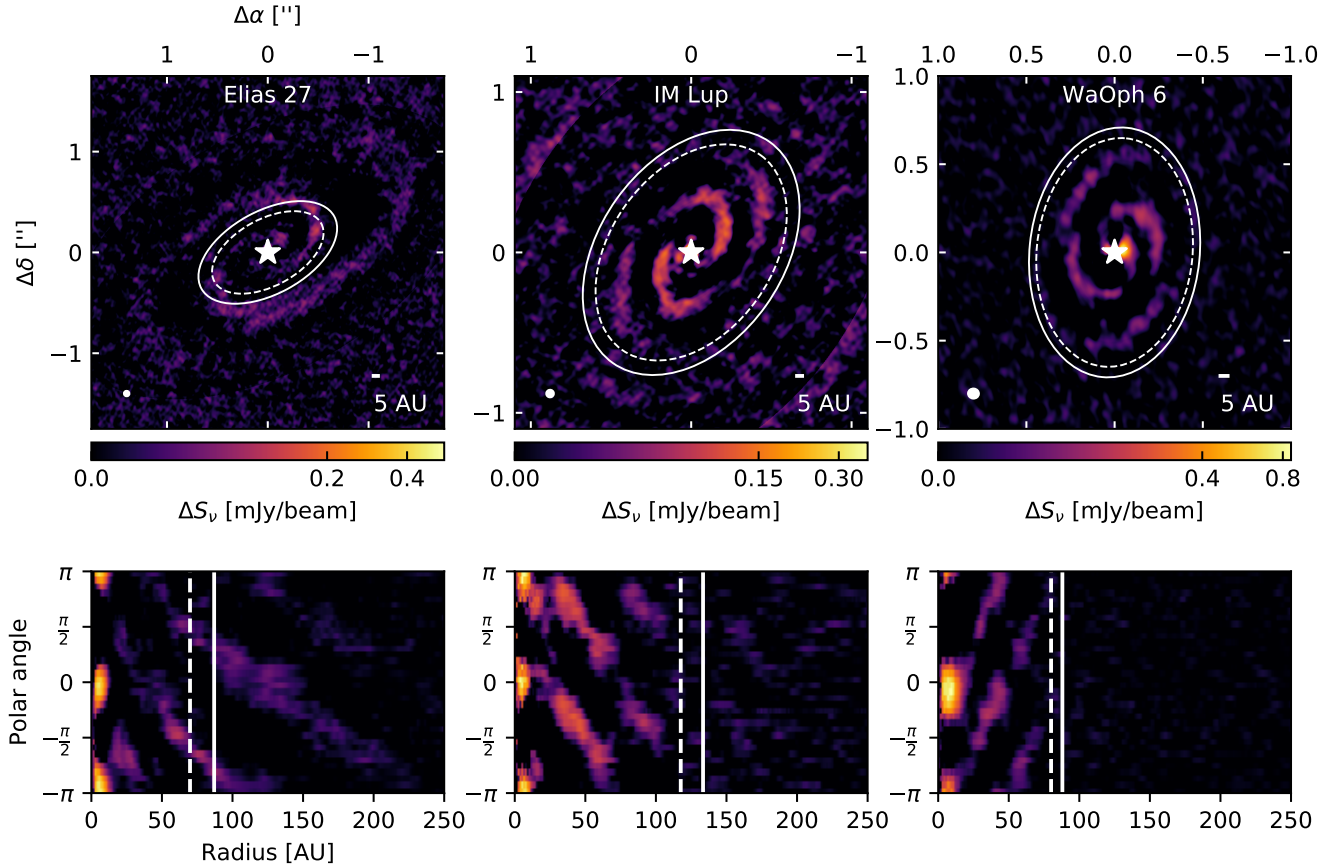


Figure 2. *Top:* Maps of the continuum emission levels above the median radial intensity profile for the Elias 27, IM Lup, and WaOph 6 disks. Note that IM Lup is shown on a smaller scale compared to Figure 1 in order to show more of the spiral detail. The white stars mark the location of the original continuum emission peaks. The dashed ellipses mark the locations of the annular gaps and the solid ellipses mark the locations of the bright rings identified in DSHARP2. The synthesized beam is shown in the lower left corner of each panel. *Bottom:* The maps in the top row deprojected and replotted as a function of radius and polar angle. The dashed vertical lines mark the locations of the annular gaps and the solid vertical lines mark the locations of the bright rings identified in DSHARP2.

different spiral forms, we prefer the simpler parametrization of the Archimedean spiral. The modeling is performed in a manner analogous to that of the logarithmic spiral fitting.

Because of the wide range of radii spanned by the spiral pattern in the Elias 27 disk and the low signal-to-noise at large radii,

The posterior medians and uncertainties computed from the 16th and 84th percentiles for R_0 and b , as well as the derived pitch angle, are listed in Table 1.

For the IM Lup disk, the spiral arm positions are measured every 20° between $R = 25$ and 75 AU and then every 6° from $R = 75$ to 110 AU (with the chosen radial breakpoint corresponding to the location of the apparent discontinuity). The spiral arm appearing to end on the northwest side of the disk is labeled “S1” and the spiral arm appearing to end on the southeast side is labeled “S2.” The portions of the arms interior and exterior to $R = 75$ AU are labeled “a” and “b,” respectively.

For the WaOph 6 disk, the spiral arm positions are measured every 18° between $R = 25$ and 50 AU and then every 9° from $R = 50$ to 80 AU (with the chosen radial breakpoint corresponding to the location of the apparent discontinuity). The spiral arm appearing to end on the north side of the disk is labeled “S1” and the spiral arm appearing to end on the south side is labeled “S2.” The results of the logarithmic spiral arm fits are listed in Table 1 and plotted in Figure 6. The results of the Archimedean spiral arm fits are listed in Table 2 and plotted in Figure 7. For the most part, the arms appear to be reasonably well-described by either logarithmic or Archimedean spirals, except that just inward and outward of the radial discontinuity identified at ~ 50 AU, a few of the measured positions appear to be following a radially constant pattern. This may be related to the presence of additional substructure discussed in 3.1, and introduces some complexity to the pitch angle calculation because radial substructure can

Table 1. Logarithmic spiral fit parameters

| Source | Feature | Polar angles fitted ^a | R_0 | b | Pitch angle |
|----------|---------|---|---------------------------------|----------------|--------------|
| | | | (AU) | | |
| Elias 27 | S1 | -112° to -28°, 29° to 133° | 114.0 ± 0.6 | -0.285 ± 0.004 | |
| Elias 27 | S2 | -151° to -47°, 68° to 152° (-292° to -208°) | 41.5 ± 0.7 | -0.296 ± 0.004 | |
| IM Lup | S1a | 70° to 170° | 91 ⁺¹¹ ₋₉ | -0.39 ± 0.06 | 21° ± 3° |
| IM Lup | S1b | -102° to 0° | 75.4 ± 1.6 | -0.175 ± 0.018 | 10° ± 1° |
| IM Lup | S2a | -110° to -10° | 30 ⁺³ ₋₂ | -0.34 ± 0.06 | 19° ± 3 |
| IM Lup | S2b | 78° to 180° (-282° to -180°) | 43 ± 3 | -0.181 ± 0.018 | 10° ± 1° |
| WaOph 6 | S1 | -112° to 104° | 45.9 ± 0.9 | 0.241 ± 0.015 | 13°.5 ± 0°.8 |
| WaOph 6 | S2 | 68° to -176° (68° to 284°) | 21.7 ± 1.4 | 0.236 ± 0.016 | 13°.3 ± 0°.8 |

^aIf applicable, the phase-unwrapped polar angle range is given in parentheses.

Table 2. Archimedean spiral fit parameters

| Source | Feature | Polar angles fitted ^a | a | c |
|---------|---------|----------------------------------|------------|-------------|
| | | | (AU) | (AU) |
| IM Lup | S1 | -102° to 170° | 73.9 ± 0.7 | -15.8 ± 0.5 |
| IM Lup | S2 | 78° to -170° (-282° to -10°) | 26.5 ± 1.7 | -15.5 ± 0.5 |
| WaOph 6 | S1 | -112° to 104° | 47.9 ± 0.8 | 11.6 ± 0.7 |
| WaOph 6 | S2 | 68° to -176° (68° to 284°) | 12 ± 2 | 11.2 ± 0.7 |

^aIf applicable, the phase-unwrapped polar angle range is given in parentheses.

create the appearance of a flattening pitch angle (and conversely, spiral structure with a flattening pitch angle can create the appearance of radial substructure). The pitch angle derived from fitting logarithmic spirals is similar to the pitch angles derived in the outer disk from fitting Archimedean spirals, but the Archimedean spiral fit suggests that the pitch angle in the inner disk could be much higher than implied by the logarithmic fit. However, In either case, The results of both fits indicate that the arms are symmetric

-address ambiguity in IM Lup (is the pitch angle of the spiral changing or are the arms just merging into the ring?)

-comment that pitch angle measurements should be interpreted very carefully, especially at lower angular resolution Any efforts to compare pitch angles measured in simulations to the pitch angles quoted here will need to take into account how the presence of multi-ring substructure or spur features may affect the inferred pitch angles.

4. DISCUSSION

4.1. Comparison to spiral arm observations in other disks

4.1.1. Spiral arms detected in millimeter continuum

So far, three other disks have had spiral features confirmed in millimeter continuum: MWC 758 (Boehler et al. 2018; Dong et al. 2018b), AS 205, and HT Lup (Kurtovic et al. in prep). So far, spiral arms in millimeter continuum have tended to be identified around later spectral types, with five out of six being found in disks hosted by K or M-type stars. However, selection bias may be at play here. The majority of disks observed at high angular resolution, as well as the majority of disks with observed spirals, originate from DSHARP, which predominantly targeted K and M stars.

The five disks hosted by K and M stars all feature $m = 2$ spiral patterns (although, as noted in section 3.1, this does not mean that there are necessarily only two arms present). The case of MWC 758 is more complicated—the millimeter continuum emission overall is highly asymmetric, but at least one spiral arm is detected on the southeast side of the disk and there are hints of another arm on the northwest side of the

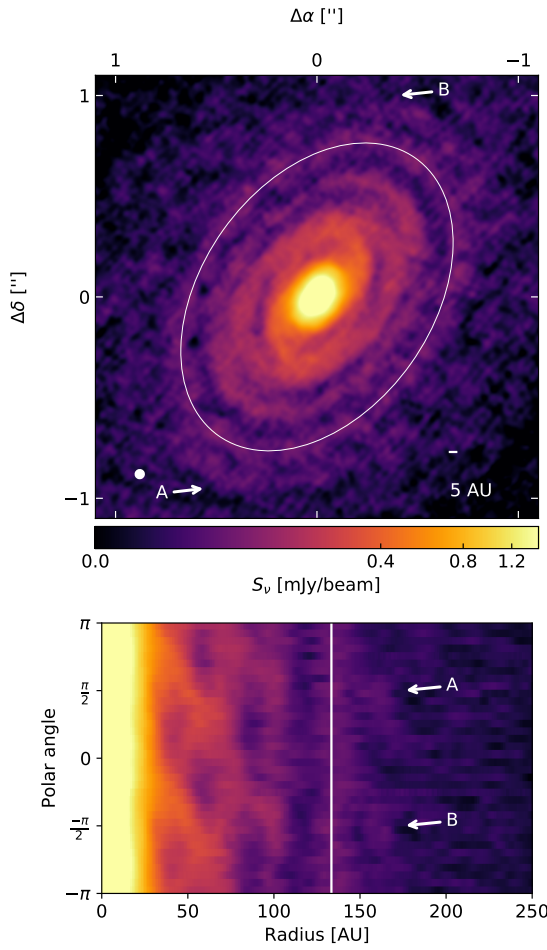


Figure 3. ALMA 1.3 mm continuum image of IM Lup and corresponding polar angle-radius plot with arrows pointing at additional substructure outside the bright ring at ~ 133 AU (marked with an ellipse in the top panel and a vertical line in the bottom panel). This substructure may be an additional pair of spiral arms, a continuation of the spiral arms interior to BR133, or another emission ring. Note that the color scale saturates at less than the peak intensity value to allow for the fainter structures to be viewed more clearly.

disk that could make up an $m = 2$ spiral pattern, although ambiguity is introduced by the disk asymmetries (Boehler et al. 2018; Dong et al. 2018b). Scattered light observations of the MWC 758, however, do reveal an $m = 2$ spiral pattern in the upper layers of the disk (Grady et al. 2013).

The dominance of $m = 2$ spiral patterns in millimeter continuum observed so far could be due at least in part to the ambiguities involved in identifying single arm systems. For example, Kraus et al. (2017) identify a “bridge” structure connecting an inner ring and outer crescent in the millimeter continuum of V1247 Ori that

appears to coincide with a spiral arm identified in scattered light, but stop short of identifying the millimeter feature itself as a spiral arm. Likewise, the crescent and ring in the 0.87 millimeter continuum of SAO 206462 (HD 135344B) also display hints of being connected at the location of a spiral arm identified in scattered light, but the angular resolution was not sufficient to be definitive (van der Marel et al. 2016).

One apparent difference between the spiral arms detected so far in multiple disk systems (AS 205 and HT Lup) and arms detected in single disk systems (MWC 758, HT Lup, IM Lup, and Elias 27) is that the former do not have clear signatures of gap and ring structure coexisting with spiral structures in the same disk, while the latter all do. So far, no obvious pattern emerges for the relative locations of the spiral and axisymmetric substructures, except that the axisymmetric substructures occur in close proximity to or even intersect with the spiral arms.

4.1.2. Observations in scattered light

Spiral arms have been detected in scattered light in at least BLANK protoplanetary disks: V1247 Ori (Ohta et al. 2016). Thus, detections in scattered light are more plentiful than detections in millimeter continuum (Discuss why)

-Ruobing’s new overview paper

-AB Aur (Hashimoto et al. 2011), HD 142527 (Casassus et al. 2012), SAO 206462 (Muto), MWC 758 (Grady et al. 2013, Benisty et al. 2015), HD 100546 (Boccaletti et al. 2013, Follette et al. 2017) HD 100453 (Wagner 2015, Benisty 2017), Oph IRS 48 is tentative (Follette et al. 2015) **(Author note: Am I missing any disks?)**

-comment on pitch angles, number of arms

-Scattered light observations are all transition disks around early type stars vs. “full” T Tauri disks in the millimeter sample. To date there have been no confirmed spiral arm detections in scattered light for K and M stars (IM Lup is ambiguous)

-Comment that ALMA observations of disks with scattered light spirals often look quite different

4.2. How common are spiral arms in protoplanetary disks?

-Spirals seem rarer than rings so far, but could be due to sensitivity/angular resolution requirements? Note the relatively modest contrast of spiral arms compared to some observed ring structures

-Impact of selection bias; if the origins are gravitational instability, then spirals would be even rarer among the smaller disks? Not sure what direction things will go in if the structures are companion-induced.

4.3. Possible origins of spiral structure

4.3.1. Companion-induced structure

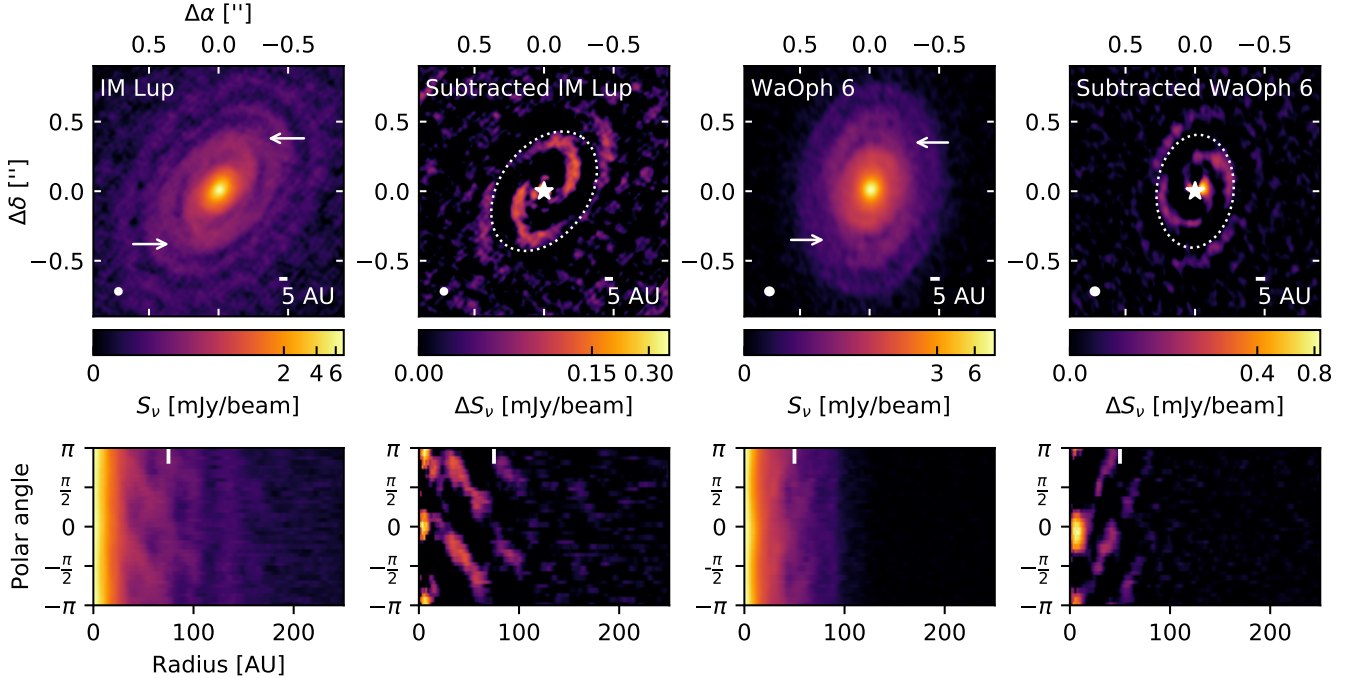


Figure 4.

Discuss Goldreich and Tremaine 1979, Bae and Zhu 2018 issues with trapping? Can we put even rough upper limits on the masses of companions?

4.3.2. Gravitational instability

-Discuss previous mass estimates (Cleeves et al. 2016, Perez et al. 2016) - generally suggest these disks are gravitationally stable, but masses might be higher for different assumptions?

-Discuss Zhu et al. 2012, Meru et al 2017, Forgan et al. 2018

4.3.3. Other hypotheses

Illumination?

5. SUMMARY

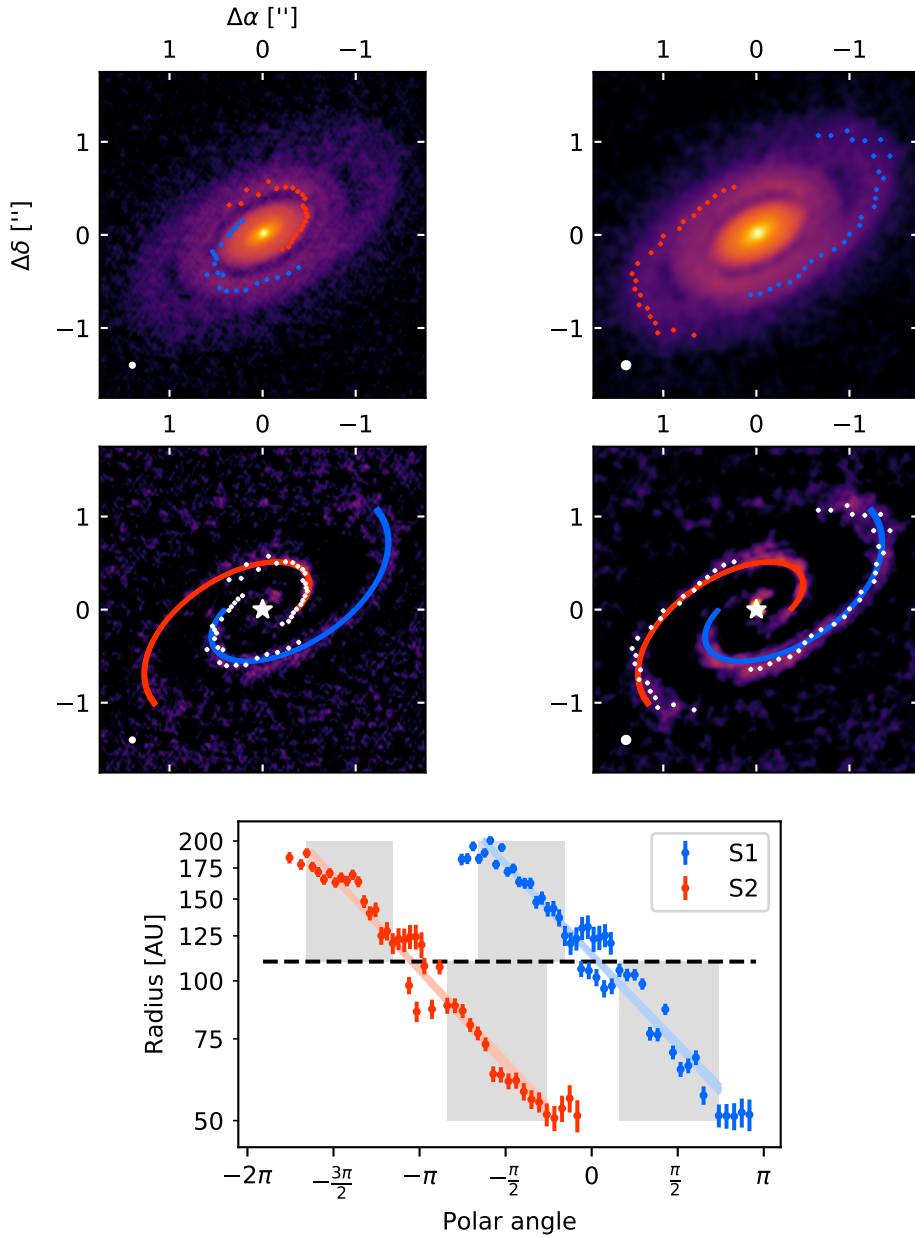
This paper makes use of ALMA data [ADS/JAO.ALMA#2016yCat.00484L](https://adsabs.harvard.edu/abs/2016yCat.00484L). We thank the NAASC and JAO staff for their advice on

data calibration and reduction. ALMA is a partnership of ESO (representing its member states), NSF (USA) and NINS (Japan), together with NRC (Canada) and NSC and ASIAA (Taiwan), in cooperation with the Republic of Chile. The Joint ALMA Observatory is operated by ESO, AUI/NRAO and NAOJ. The National Radio Astronomy Observatory is a facility of the National Science Foundation operated under cooperative agreement by Associated Universities, Inc. J.H. acknowledges support from the National Science Foundation Graduate Research Fellowship under Grant No. DGE-1144152 and from NRAO Student Observing Support.

Software: `analysisUtils` (https://casaguides.nrao.edu/index.php/Analysis_Utils), `AstroPy` (Astropy Collaboration et al. 2013), `CASA` (McMullin et al. 2007), `emcee` (Foreman-Mackey et al. 2013), `matplotlib` (Hunter 2007), `scikit-image` (van der Walt et al. 2014), `SciPy` (Jones et al. 2001)

REFERENCES

- Alcalá, J. M., Manara, C. F., Natta, A., et al. 2017, A&A, 600, A20
- Astropy Collaboration, Robitaille, T. P., Tollerud, E. J., et al. 2013, A&A, 558, A33
- Avenhaus, H., Quanz, S. P., Garufi, A., et al. 2018, ArXiv e-prints, arXiv:1803.10882
- Boehler, Y., Ricci, L., Weaver, E., et al. 2018, ApJ, 853, 162
- Cleeves, L. I., Öberg, K. I., Wilner, D. J., et al. 2016, ApJ, 832, 110
- Dong, R., Najita, J. R., & Brittain, S. 2018a, ArXiv e-prints, arXiv:1806.05183
- Dong, R., Liu, S.-y., Eisner, J., et al. 2018b, ApJ, 860, 124
- Eisner, J. A., Hillenbrand, L. A., White, R. J., Akeson, R. L., & Sargent, A. I. 2005, ApJ, 623, 952

**Figure 5.**

- Elmegreen, D. M. 1980, ApJ, 242, 528
 Foreman-Mackey, D., Hogg, D. W., Lang, D., & Goodman, J. 2013, Publications of the Astronomical Society of the Pacific, 125, 306
 Fukagawa, M., Hayashi, M., Tamura, M., et al. 2004, ApJL, 605, L53
 Gaia Collaboration, Brown, A. G. A., Vallenari, A., et al. 2018, ArXiv e-prints, arXiv:1804.09365
 Goldreich, P., & Tremaine, S. 1979, ApJ, 233, 857

- Goodman, J., & Weare, J. 2010, Communications in Applied Mathematics and Computational Science, 5, 65
 Grady, C. A., Muto, T., Hashimoto, J., et al. 2013, ApJ, 762, 48
 Hunter, J. D. 2007, Computing In Science & Engineering, 9, 90
 Jones, E., Oliphant, T., Peterson, P., et al. 2001, SciPy: Open source scientific tools for Python, ,
 Kraus, S., Kreplin, A., Fukugawa, M., et al. 2017, ApJ, 848, L11

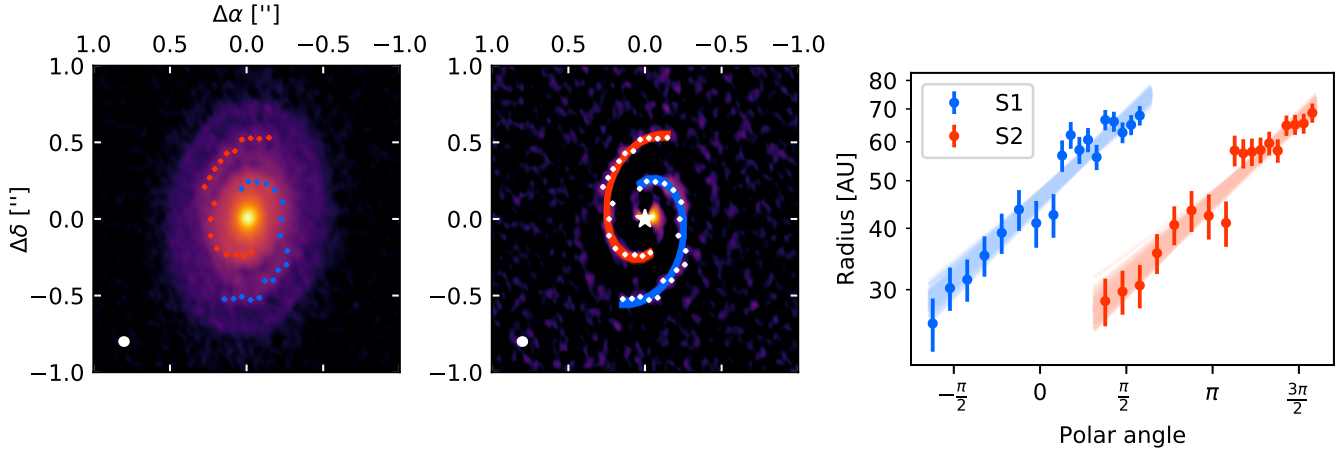


Figure 6. Comparisons of logarithmic spiral arm fits to the WaOph 6 data. *Left:* Measured positions of the spiral arms plotted as orange (S1) and blue (S2) markers over the 1.3 millimeter continuum image. *Middle:* Measured spiral positions (white markers) and logarithmic spirals derived from 100 random draws from each posterior (orange and blue) plotted over the continuum image with axisymmetric emission subtracted. *Right:* Measured spiral positions with 1σ error bars compared with logarithmic spirals derived from 100 random draws from the posterior for each arm. Note that the y-axis is on a log-scale and the position of S2 is plotted using the unwrapped polar angle values in order to maintain continuity.

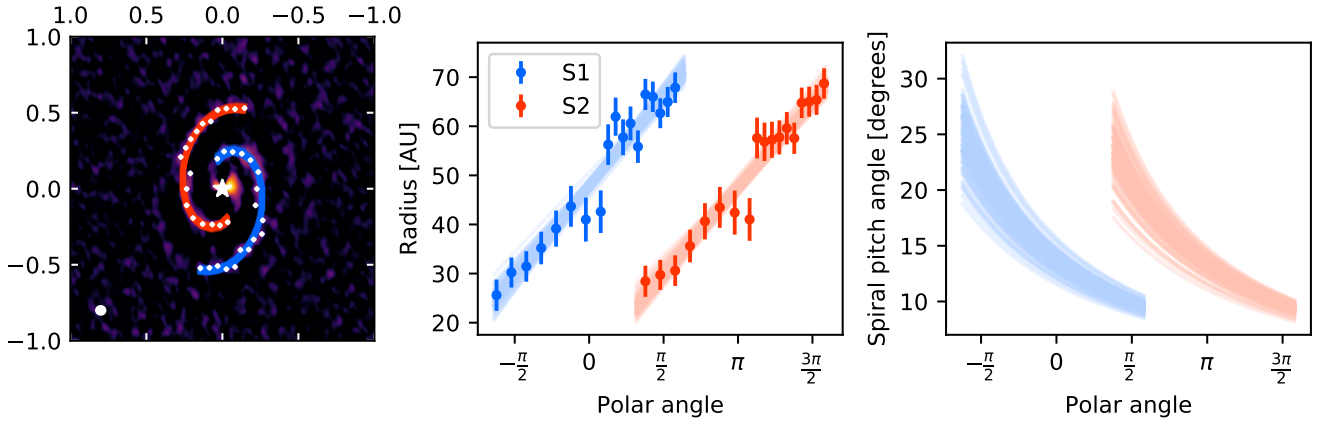


Figure 7. Comparisons of Archimedean spiral arm fits to the WaOph 6 data. *Left:* Measured spiral positions (white markers) and Archimedean spirals derived from 100 random draws from each posterior (orange and blue) plotted over the continuum image with axisymmetric emission subtracted. *Middle:* Measured spiral positions with 1σ error bars compared with Archimedean spirals derived from 100 random draws from the posterior for each arm. Note that the y-axis is on a linear-scale and the position of S2 is plotted using the unwrapped polar angle values in order to maintain continuity. *Right:* Pitch angles derived from 100 random draws from the posterior, plotted as a function of polar angle.

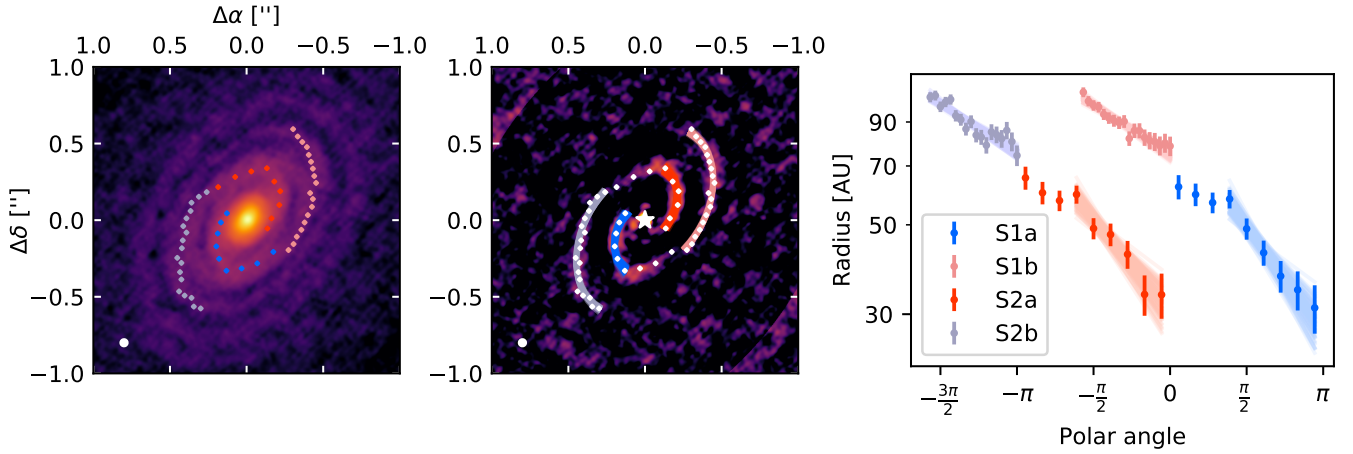


Figure 8. Comparisons of logarithmic spiral arm fits to the IM Lup data. *Left:* Measured positions of the spiral arms plotted as orange (S1a), blush (S2b), blue (S2a), and lavender (S2b) markers over the 1.3 millimeter continuum image. *Middle:* Measured spiral positions (white markers) and logarithmic spirals derived from 100 random draws from each posterior (orange, blush, blue, and lavender) plotted over the continuum image with axisymmetric emission subtracted. *Right:* Measured spiral positions with 1σ error bars compared with logarithmic spirals derived from 100 random draws from the posterior for each arm. Note that the y-axis is on a log-scale and the position of S2 is plotted using the unwrapped polar angle values in order to maintain continuity.

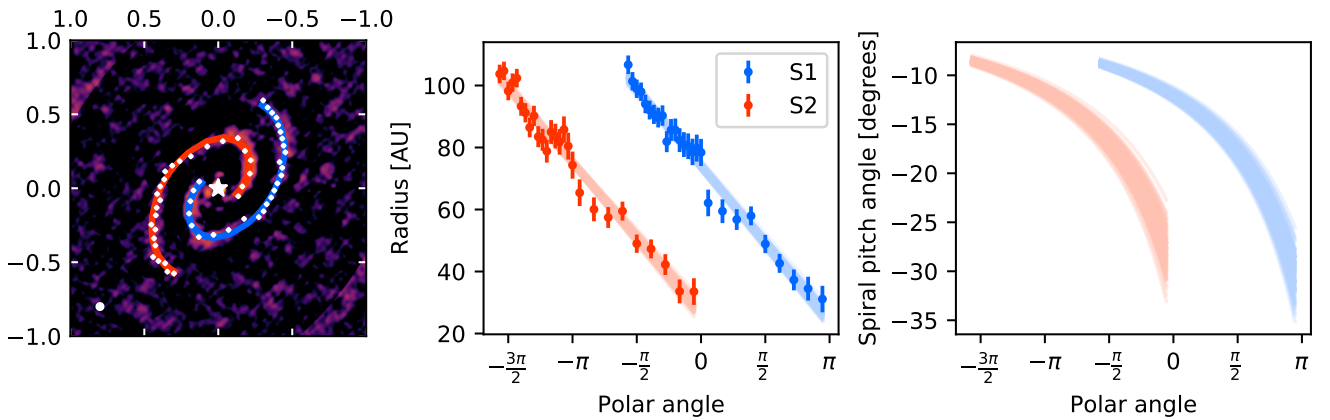


Figure 9. Similar to Figure 7, but for the IM Lup disk.

- Lodato, G., & Rice, W. K. M. 2004, MNRAS, 351, 630
- Luhman, K. L., & Rieke, G. H. 1999, ApJ, 525, 440
- Mayer, L., Quinn, T., Wadsley, J., & Stadel, J. 2004, ApJ, 609, 1045
- McMullin, J. P., Waters, B., Schiebel, D., Young, W., & Golap, K. 2007, in Astronomical Society of the Pacific Conference Series, Vol. 376, Astronomical Data Analysis Software and Systems XVI, ed. R. A. Shaw, F. Hill, & D. J. Bell, 127
- Montesinos, M., & Cuello, N. 2018, MNRAS, 475, L35
- Montesinos, M., Perez, S., Casassus, S., et al. 2016, ApJ, 823, L8
- Muto, T., Grady, C. A., Hashimoto, J., et al. 2012, ApJL, 748, L22
- Ohta, Y., Fukagawa, M., Sitko, M. L., et al. 2016, PASJ, 68, 53
- Pérez, L. M., Carpenter, J. M., Andrews, S. M., et al. 2016, Science, 353, 1519
- Pinte, C., Padgett, D. L., Ménard, F., et al. 2008, A&A, 489, 633
- Rafikov, R. R. 2002, ApJ, 569, 997
- Rosenfeld, K. A., Andrews, S. M., Hughes, A. M., Wilner, D. J., & Qi, C. 2013, ApJ, 774, 16
- Tanaka, H., Takeuchi, T., & Ward, W. R. 2002, ApJ, 565, 1257
- van der Marel, N., Cazzoletti, P., Pinilla, P., & Garufi, A. 2016, ApJ, 832, 178
- van der Walt, S., Schönberger, J. L., Nunez-Iglesias, J., et al. 2014, PeerJ, 2, e453
- Zhu, Z., Dong, R., Stone, J. M., & Rafikov, R. R. 2015, ApJ, 813, 88

Facilities: ALMA